Structural Studies of a Crystalline Insulin Analog Complex with Protamine by Atomic Force Microscopy

Christopher M. Yip*, Mark L. Brader*, Bruce H. Frank*, Michael R. DeFelippis*, and Michael D. Ward[†]

*Lilly Research Laboratories, Eli Lilly and Company, Indianapolis, Indiana 46285 and [†]Department of Chemical Engineering and Materials Science and the Center for Interfacial Engineering, University of Minnesota, Minneapolis, Minnesota 55455 USA

ABSTRACT   Crystallographic studies of insulin–protamine complexes, such as neutral protamine Hagedorn (NPH) insulin, have been hampered by high crystal solvent content, small crystal dimensions, and extensive disorder in the protamine molecules. We report herein in situ tapping mode atomic force microscopy (TMAFM) studies of crystalline neutral protamine $Lys^{B28}Pro^{B29}$ (NPL), a complex of $Lys^{B28}Pro^{B29}$ insulin, in which the C-terminal prolyl and lysyl residues of human insulin are inverted, and protamine that is used as an intermediate time-action therapy for treating insulin-dependent diabetes. Tapping mode AFM performed at 6°C on bipyramidally tipped tetragonal rod-shaped NPL crystals revealed large micron-sized islands separated by 44-Å tall steps. Lattice images obtained by in situ TMAFM phase and height imaging on these islands were consistent with the arrangement of individual insulin–protamine complexes on the $P4_12_12$ (110) crystal plane of NPH, based on a low-resolution x-ray diffraction structure of NPH, arguing that the NPH and NPL insulins are isostructural. Superposition of the height and phase images indicated that tip-sample adhesion was larger in the interstices between NPL complexes in the (110) crystal plane than over the individual complexes. These results demonstrate the utility of low-temperature TMAFM height and phase imaging for the structural characterization of biomolecular complexes.

INTRODUCTION

The treatment of diabetes often requires regular injections of insulin, a 51-amino-acid dual chain polypeptide hormone secreted by the pancreas (Banting and Best, 1922; Brange, 1987). Stored as a Zn^{2+}-hexamer in the pancreas, insulin binds as a monomer with its transmembrane receptor. To mimic normal physiologic insulin levels, numerous therapeutic insulin formulations have been devised, including rapid-acting monomeric insulin analogues and extended time-action therapies based on crystalline insulin forms. Intermediate-acting therapies typically are administered as mixtures of crystalline and amorphous forms of insulin or cocrystalline insulin complexes prepared with protamine (Krayenbuhl and Rosenberg, 1946). A highly basic polypeptide composed of primarily arginine residues, protamine is isolated from fish sperm and most often used clinically in cardiovascular surgery because it can neutralize the effect of heparin (Weiler et al., 1985).

Known as neutral protamine Hagedorn (NPH) (Hagedorn et al., 1936), these cocrystalline complexes can be prepared identically from wild-type human, beef, or pork insulins because all these insulin forms possess similar self-association properties and readily form hexamers in the presence of zinc (Goldman and Carpenter, 1974; Pekar and Frank, 1972). Unfortunately, crystallographic studies have provided only a low-resolution structure for a wild-type pork insulin complex with clupeine Z, a highly purified form of protamine (Balschmidt et al., 1991; Baker and Dodson, 1970; Simkin et al., 1969; Fullerton and Low, 1970).

A key step in insulin binding and receptor activation is insulin multimer dissociation to the bioactive monomer (Hollenberg, 1990; Smith et al., 1984; Brange, 1991). Consequently, recent efforts to devise more effective insulin-based therapies have focused on manipulating insulin's self-association (or dissociation) properties (Brange et al., 1991). The insulin analogue, $Lys^{B28}Pro^{B29}$, which bears a single site sequence inversion at positions 28 and 29 in the human insulin B-chain, is illustrative of efforts in this regard (Brems et al., 1992; Long et al., 1992; DiMarchi et al., 1992). With a 300-fold reduction in the monomer–dimer association constant relative to human insulin, $Lys^{B28}Pro^{B29}$ is an excellent candidate as a rapid-acting diabetes therapy. Despite the tendency for $Lys^{B28}Pro^{B29}$ to exist in a monomeric form, it can be crystallized in the presence of phenolic ligands and zinc as a hexameric zinc complex resembling wild-type insulins (Ciszak et al., 1995; Bakaysa et al., 1996; Birnbaum et al., 1997). This close structural correspondence resulted in the development of a $Lys^{B28}Pro^{B29}$-based analog of NPH insulin known as neutral protamine $Lys^{B28}Pro^{B29}$ (NPL), which was recently shown to be an effective intermediate time-action diabetes therapy (DeFelippis et al., 1998).

The physical properties of crystalline materials can be influenced by various factors including crystal polymorphism, morphology, and size. In the case of therapeutic complexes, the convenient direct characterization of the local crystal–solution interface can provide key insights into the relationship(s) between molecular orientation, surface morphology, interfacial structure, and efficacy. Because NPL insulins are administered as microcrystalline suspensions for the treatment of diabetes, atomic force microscopy

(AFM) studies of the crystal interface can provide insights into the factors specific to NPL crystal dissolution and bioavailability. We and others have demonstrated the suitability of AFM for studying interfacial structure, including direct real-space resolution of crystal lattice periodicities and in situ confirmation of space group symmetries for molecular crystals (Hillier and Ward, 1994; Carter et al., 1994), and crystals of insulin (Yip and Ward, 1996; Yip et al., 1998a,b) and other proteins (Durbin and Carlson, 1992; Malkin et al., 1995, 1996; McPherson et al., 1996; Durbin et al., 1993; Konnert et al., 1994; Land et al., 1995, 1996; Walz et al., 1996; Li et al., 1999a,b).

We describe herein the results of an in situ tapping mode AFM (TMAFM) study of NPL crystals performed in crystallization liquor. Imaging performed during crystallization over extended periods of time revealed that NPL growth proceeded by the nucleation of two-dimensional (2D) islands and their subsequent expansion. In situ AFM imaging of the prominent exposed faces of NPL crystals revealed lattice parameters identical to those expected for the (110) face of NPH crystals, indicating that NPL and NPH crystals are isostructural. (Balschmidt et al., 1991). These results also demonstrate that TMAFM phase imaging, which was used to acquire the in situ images of the NPL crystals, can identify temperature-dependent protein crystallization mechanisms, and enable assignment of plausible crystallographic structures for protein complexes.

MATERIALS AND METHODS

Following the procedure described by Balschmidt et al., crystals of NPL were prepared from urea-containing crystallization liquors at urea concentrations ranging from 1 M to 4 M (Balschmidt et al., 1991). The procedure for the 4 M urea crystallization is as follows. To a 100-ml Erlenmeyer flask containing 194.55 mg of $Lys^{B28}Pro^{B29}$ (Eli Lilly and Company, Indianapolis, IN) and 0.569 mg ZnO, was added 25 ml of 4 M urea, 27 mM phosphoric acid, 21 mM m-cresol, and 120 mM NaCl buffer. After gentle swirling to dissolve the $Lys^{B28}Pro^{B29}$, the solution pH was adjusted to 7.3 with dilute sodium hydroxide solution. In a similar manner, 18 mg of protamine sulfate (Yuki Gosei, Tokyo, Japan) was dissolved in 25 ml of the same urea buffer solution (4 M urea, 27 mM phosphoric acid, 21 mM m-cresol, and 120 mM NaCl) to yield a clear solution. The pH of the protamine solution was adjusted to 7.3 with dilute sodium hydroxide solution. After thermal equilibration at room temperature, 2 ml of the $Lys^{B28}Pro^{B29}$ solution was added to a 25-ml glass scintillation vial. An equal volume of the protamine solution was added to yield a clear solution. Well-formed millimeter-sized bipyramidally tipped tetragonal rod crystals grew from clear solution over the course of several days at ambient 23°C temperatures. Crystallizations performed at 6°C yielded smaller, fragmented, stellate clusters of crystals.

All solution tapping atomic force microscopy images were acquired using a combination contact/tapping mode liquid cell fitted to a Nanoscope IIIA MultiMode scanning probe microscope (Digital Instruments, Santa Barbara, CA). All images were acquired using 120 μm oxide-sharpened silicon nitride V-shaped cantilevers (Type DNP-S, Digital Instruments). Before use, the AFM tips were exposed to ultraviolet irradiation to remove adventitious organic contaminants from the tip surface. The AFM images were acquired using the E scanning head, which has a maximum lateral scan area of 14.6 [mult] 14.6 μm. In situ imaging was performed on crystals that had been transferred via pipette from the crystallization vial into a small circular cell defined by an O-ring placed on a magnetic AFM mount. The AFM mount was previously coated with a thin layer of vacuum grease to affix the crystal and prevent its movement during scanning. The AFM liquid cell was then placed carefully over the O-ring and the AFM tip positioned using an in-line optical microscope that permitted simultaneous viewing of the AFM tip and the crystal surface of interest. Once seated on the O-ring, the liquid cell has restricted lateral translation, which makes it important to minimize the need for tip positioning. We have found the following procedure to be effective in reliably locating and positioning the AFM tip. The cantilever is inserted into the AFM liquid cell and the laser spot aligned on the cantilever tip. The liquid cell is then removed from the AFM optical head and replaced with the AFM magnetic mount containing the crystals of interest. Without adjusting the laser spot positioning screws and while monitoring the position of the laser spot through an optical microscope, the AFM optical head is translated in the X–Y plane until the laser spot is located above a crystal of interest. The liquid cell containing the premounted cantilever tip is then reseated over the O-ring. Optimal tapping mode imaging was achieved at a cantilever drive frequency of ~8.9 kHz. The cantilever drive and setpoint voltages were found to play a significant role in determining image quality and sample integrity because slight deviations from the optimal feedback conditions led to diminished resolution and sample etching.

Low temperature AFM imaging was accomplished by placing the entire AFM base inside a thermoelectric refrigeration unit (Igloo—36 qt). This approach alleviated the mechanical and electronic interference associated with conventional compressor-driven refrigeration. For these experiments, the laser spot was aligned on the cantilever tip and an initial AFM image acquired to ensure proper tip–sample engagement. The AFM tip was then withdrawn from the sample surface a distance of 5 μm and the entire unit placed in the refrigeration unit. The entire system was allowed to reach thermal equilibrium before reinitiating AFM imaging. The temperature in the refrigeration unit was recorded with an Omega HH82 digital thermometer fitted with a K-type thermocouple. Vertical and lateral calibration of the piezoelectric scanner at the two operating temperatures was accomplished by acquiring real-space 2D lattice periodicities on the exposed basal planes of freshly cleaved mica and graphite.

RESULTS AND DISCUSSION

The crystallization of $Lys^{B28}Pro^{B29}$ with protamine from urea-containing crystallization buffers yielded well-defined crystals with morphologies and dimensions that were dependent on the concentration of the urea in the crystallization liquor and the crystallization temperature. The $Lys^{B28}Pro^{B29}$—protamine cocrystals grew at room temperature from clear 4-M urea solutions as large millimeter-size bipyramidally tipped tetragonal rods similar in appearance to crystals reported for the porcine insulin-clupeine Z complex, (Balschmidt et al., 1991) (Fig. 1). At urea concentrations <4 M, mixing of the $Lys^{B28}Pro^{B29}$ and protamine solutions led to the immediate formation of a white precipitate. Both tetragonal rod and hexagonal plate crystals were formed from 3-M urea solutions, whereas a mixture of single and stellate tetragonal rod crystals formed in 1-M urea solutions. When NPL crystallization occurs from urea-free phosphate buffer solution, ~1.5 [mult] 5 μm tetragonal rod crystals form within 24 hrs at 15°C (DeFelippis et al., 1998). In all cases, crystallizations performed at 6°C resulted in crystals that were smaller and more fragmented than those obtained from ambient temperature crystalliza-
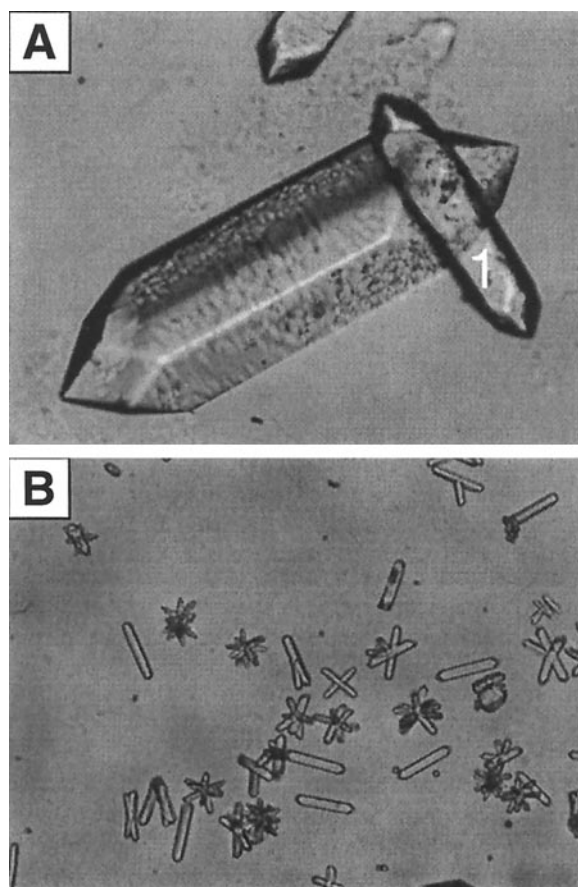
FIGURE 1 Optical micrographs of Lys^{B28}Pro^{B29}–protamine single crystals grown at (A) room temperature and (B) 6°C. Magnification: 200[mult]. In both sets of micrographs, the tetragonal rod morphology is apparent. (A) The region marked 1 indicates a typical prolate hexagonal crystal face imaged during the AFM studies. (B) Rapid crystal nucleation and growth at the lower crystallization temperature is reflected in fragmented and stellate appearance of the crystals.

tion. These differences in crystal morphology and size suggest variations in the growth rates of various crystal planes, reflecting modifications in the free energy of attachment of the prenucleation crystal aggregates to the actively growing crystal planes.

The formation of a white precipitate upon mixing of Lys^{B28}Pro^{B29} and protamine solutions suggests the rapid formation of crystal nuclei. The extent of precipitation decreased with increasing urea content in the crystallization liquor, and the crystals were larger and better defined, suggesting that urea inhibits the initial stage of Lys^{B28}Pro^{B29}–protamine association and/or the aggregation of these complexes into crystal nuclei. This is further supported by the formation of a precipitate when NPL crystallization is performed in phosphate buffer in the absence of urea, regardless of the phosphate ion concentration. Although urea is often viewed as a protein denaturant, the levels of urea used here are unlikely to induce denaturation of insulin. Numerous studies of insulin have demonstrated

its robustness to urea and other protein denaturants (Bryant et al., 1992; Brems et al., 1990). Moreover, examination of the porcine insulin-clupeine Z NPH x-ray structure and preliminary diffraction data acquired on NPL crystals prepared here did not reveal any significant conformational distortion of the constituent insulin or Lys^{B28}Pro^{B29} hexamers (G. D. Smith, personal communication).

AFM imaging

Tapping mode AFM imaging performed in crystallization liquor at ambient temperature on the large prolate hexagonal faces (Fig. 1 A, *Region 1*) of the tetragonal NPL crystals grown from 4-M urea solutions revealed large micron-sized molecularly flat terraces separated by 44 ± 6 Å steps. However, attempts to acquire molecular scale contrast by imaging over small areas or for extended times over large areas were thwarted by surface etching, despite efforts to minimize contact forces. Inspection of the crystal surface by optical microscopy performed simultaneously with AFM imaging revealed the gradual dissolution of the NPL crystal outside of the region scanned by the AFM tip. We note that the temperature of the fluid within the AFM liquid cell, measured with an in-line thermocouple, was 33°C, about 10°C higher than the surrounding room. We surmise that this slight elevation in temperature increases the solubility of the NPL crystal, and ultimately initiates crystal dissolution. Remarkably, this effect was not observed in our earlier studies of insulin and insulin analog crystallization (Yip and Ward, 1996; Yip et al., 1998a,b). Consequently, we performed in situ AFM imaging at 6°C, a condition at which crystal dissolution and surface etching was not observed on our experimental time scales. Recently, AFM imaging at low temperatures has been used successfully to study biological materials (Zhang et al., 1996; Ng et al., 1997).

Our low temperature experiments were performed by placing the AFM head inside an insulated chamber outfitted with a simple Peltier-type thermoelectric chiller. By minimizing the mechanical and electronic interference that prevented the use of conventional refrigerators, this approach enabled stable imaging at reduced temperatures. Tapping mode AFM imaging performed in crystallization liquor at 6°C on the prominent prolate hexagonal faces of the bipyramidally tipped tetragonal rod NPL crystals revealed large well-ordered crystal terraces separated by 44 ± 4-Å steps. The step heights measured at 33°C and 6°C differed by <1.0 Å, confirming that the calibration of the piezoelectric scanner was not significantly affected by the reduction in operating temperature.

Molecular level contrast obtained by height and phase imaging on the exposed crystal faces of NPL revealed an ordered lattice with real-space parameters of $a_1 = 76.0$ Å; $a_2 = 118$ Å; $a_3 = 75.2$ Å; $\gamma_{12} = 46.5°$; $\gamma_{23} = 41.3°$ (Fig. 2). These values argue that the crystal possesses *p4mm* plane group symmetry, an observation consistent with pre-
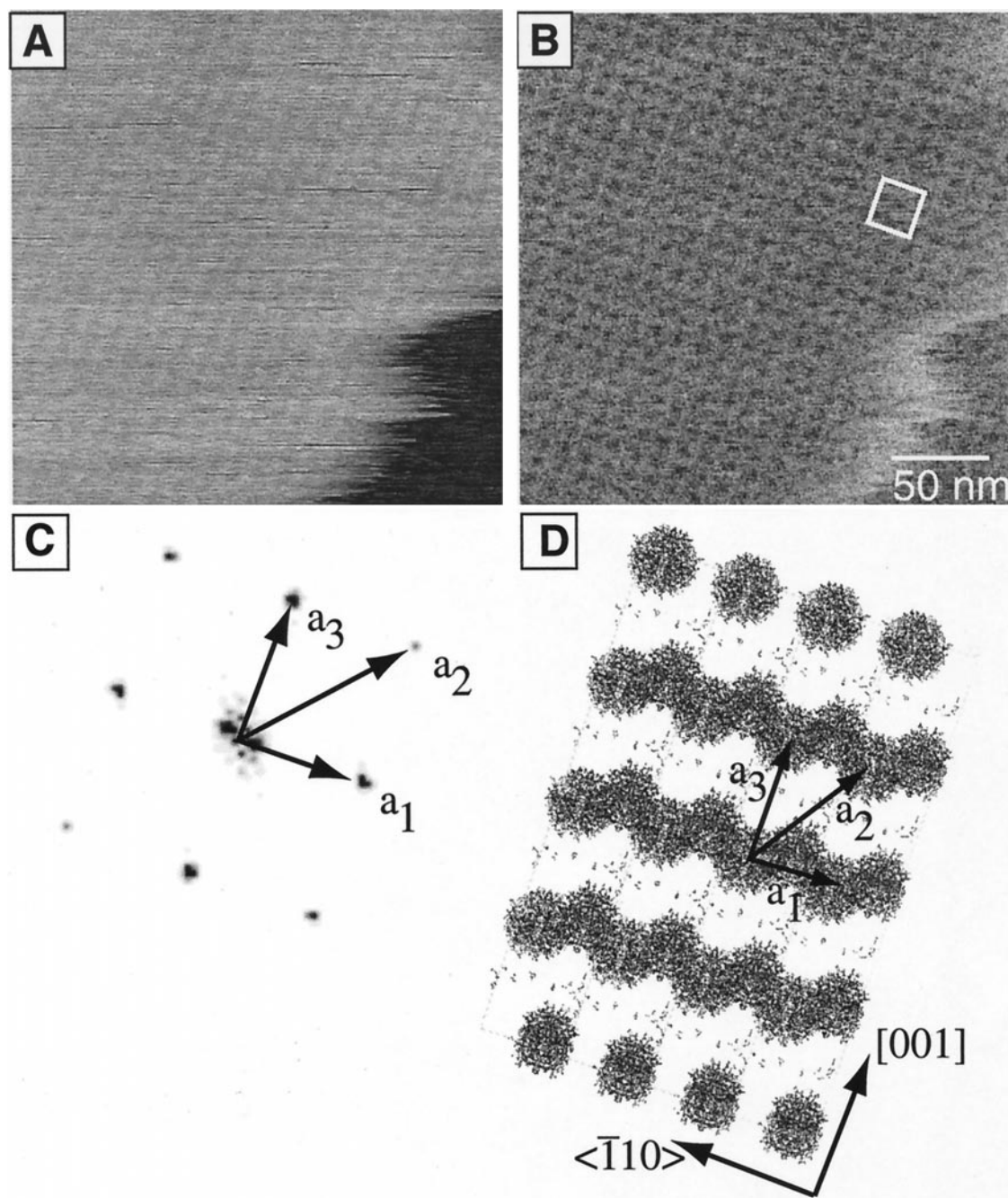
FIGURE 2   Tapping mode AFM images acquired in solution at 6°C on the prolate hexagonal face of a $Lys^{B28}Pro^{B29}$–protamine single crystal. Unfiltered (*A*) height and (*B*) phase-encoded AFM images of a large molecularly flat terrace revealing well-ordered surface periodicities. Note correspondence between height and phase image periodicities. Scan rate: 2.0 Hz. Image size: 250 nm. The AFM unit cells deduced by Fourier analysis are shown as solid white lines. (*C*) Two-dimensional Fourier power spectrum of phase image (*B*) revealing fourfold symmetry corresponding to real-space vectors $a_1 = 76.0$ Å; $a_2 = 118$ Å; $a_3 = 75.2$ Å; $\gamma_{12} = 46.5°$; $\gamma_{23} = 41.3°$. (*D*) Molecular model of the (110) crystal plane of the porcine insulin–clupeine Z complex. The model was prepared using Cerius[2] version 2.1 (Molecular Simulations Inc. San Diego CA) from coordinates registered with the Brookhaven Protein Data Bank as entry code: pdb7ins.ent.

liminary x-ray diffraction studies suggested that these crystals belong to the 4/*mmm* Laue space group (G. D. Smith, personal communication). Comparison with the porcine insulin–clupeine Z NPH complex, which belongs to the $P4_12_12$ space group (or its enantiomeric complement

$P4_32_12$) with lattice parameters $a = b = 62.9$ Å, $c = 85.9$ Å, $\alpha = \beta = \gamma = 90°$, revealed a fair correspondence between the a_1 and a_3 vectors determined by AFM and the symmetry equivalent $\langle \bar{1}11 \rangle$ (88.9 Å) and [001] (85.9 Å) lattice parameters, respectively, for the $P4_12_12$ (110) crystal
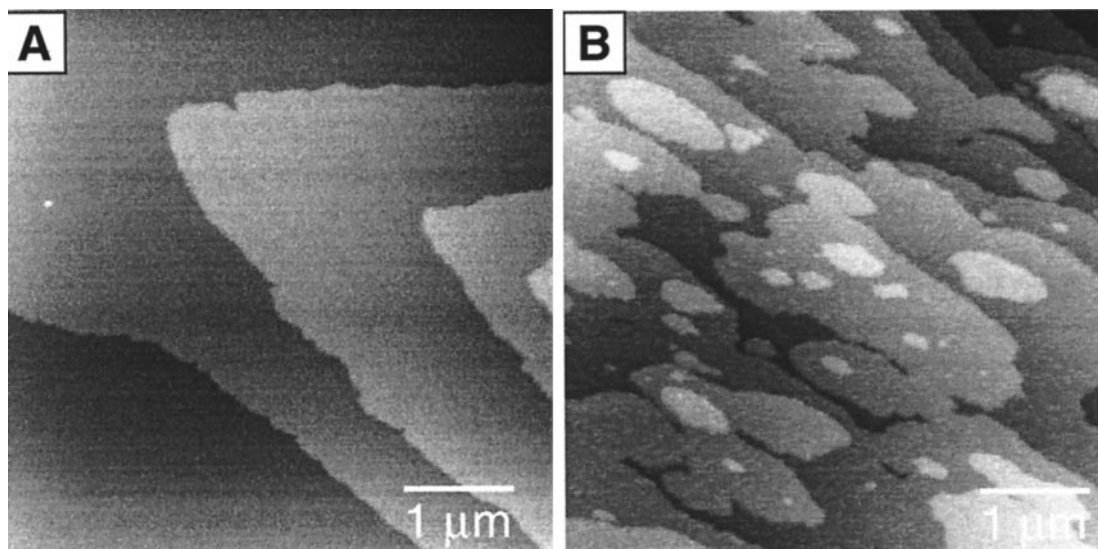
FIGURE 3   In situ tapping mode images of Lys^{B28}Pro^{B29}-protamine complex acquired at (*A*) 33°C and (*B*) 6°C. Images were acquired on the same crystal in the same region of a large prolate hexagonal crystal face. Change in surface topography supports transition from terrace expansion growth seen in (*A*) to a 2D nucleation and island expansion mechanism seen in (*B*). Image size: 5 [mult] 5 μm. Scan rate: 2.0 Hz.

plane (Balschmidt et al., 1991). The experimentally determined a_2 vector, therefore, is assigned to the symmetry equivalent $\langle \bar{1}11 \rangle$ (124 Å) lattice parameters of the NPH crystals. The small discrepancy between the AFM data for NPL and the crystallographic analysis for NPH may be due to slight reconstruction of the NPL crystal surface. Nevertheless the observed 44 Å vertical spacing between individual NPL crystal terraces is comparable to the interplanar spacing of NPH (110) planes corroborating that the NPH and NPL crystal forms are isostructural.

Phase contrast imaging

During tapping mode imaging, the AFM tip is oscillated at a user-specified frequency and drive amplitude such that the tip only contacts the sample surface intermittantly. The optimal choice of frequency and amplitude depends on the nature of the surrounding fluid, the dynamic response of the sample surface, and the mechanical coupling of the AFM liquid cell with the fluid. The AFM control loop monitors the amplitude dampening of the tip oscillation as the tip contacts the sample surface and adjusts the relative sample-tip separation accordingly. This feedback mechanism thus provides image contrast associated with constant amplitude damping by the surface. Recent reports have demonstrated that the phase shift between the applied and detected tip oscillation can provide information regarding intrinsic local surface modulus and viscoelasticity (Winkler et al., 1996; Maganov et al., 1997). Under constant amplitude imaging conditions, the applied tip force depends strongly on sample and tip stiffness, drive frequency, and sample deformation (Spatz et al., 1995). Whereas, in air, the amplitude of the tip

oscillations can be several tens of nanometers with corresponding high applied transient contact forces, tapping mode imaging performed in solution involves small tip oscillations and low setpoint amplitudes, typically <5 nm. Under these light tapping conditions, the observed phase shift presumably reflects differences in the amount of energy dissipated during tip contact with the surface (Cleveland et al. 1998). Such energy losses can arise through convolution of the mechanical properties of the surface with electrostatic forces between the tip and surface. Indeed, the extent of mechanical deformation of the individual protein domains will depend on the magnitude of the applied tip force and the viscoelastic characteristics of the protein, as reported in contact mode AFM studies of 2D protein crystals (Muller et al.; 1995).

Although the basis for the absolute phase image contrast values remains unclear, significant relative phase contrast was observed as the tip traversed over the individual Lys^{B28}Pro^{B29} hexamer–protamine complexes and the adjacent interstitial contact regions (Fig. 2 *B*). The excellent registry of the absolute phase and height regions clearly demonstrates that phase imaging can be used to acquire nanometer-scale resolution of protein crystal surfaces. In the present study, phase contrast imaging provided clearer resolution of the 2D surface lattice of the NPL crystals than the corresponding amplitude or height images, including clear delineation of the crystal terrace edges (Fig. 2 *B*).

The magnitude of the phase shift observed during TMAFM imaging in fluids can be correlated with specific adhesive interactions between the tip and surface, with the phase lag increasing with increasing adhesion, and energy dissipation (Noy et al., 1998; Brandsch et al., 1997;
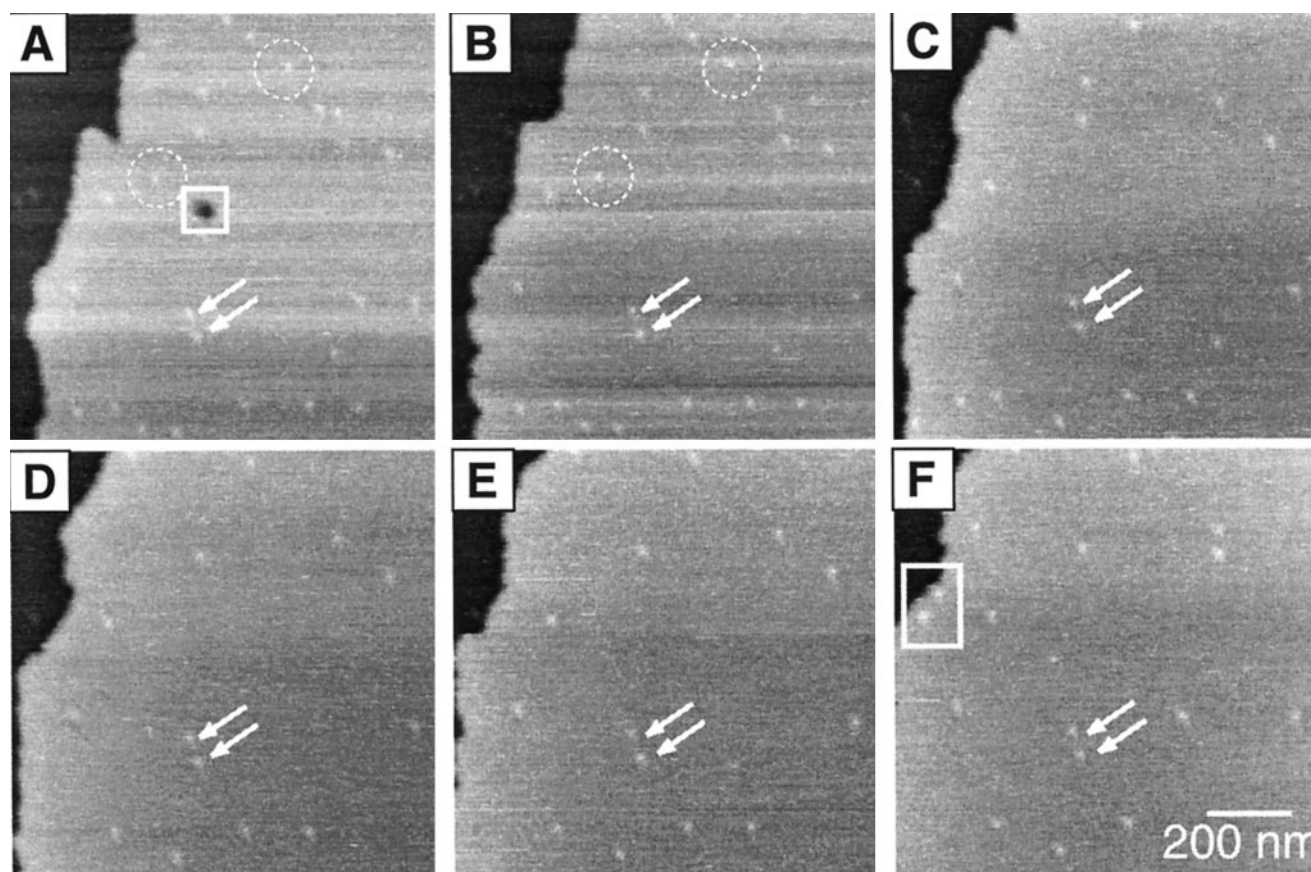
FIGURE 4 (A–F) Real-time in situ tapping mode AFM images collected at 0, 129, 515, 772, 1030, and 1416 s, respectively, in crystallization liquor at 33°C. The images reveal the active adsorption and desorption of 17 Å tall aggregates on the actively growing crystal terrace. Persistent aggregates, denoted by the white arrows, confirm the lack of image drift. (A) The white outline indicates a region where a single molecular layer deep hole has formed. Note how this region undergoes reconstruction on the time frame of <129 s, with no accompanying dislocation or crystal defect formation. The dotted white outlines in (A–B) highlight aggregates initially present on the terrace surface that have desorbed from the terrace in (C). In (F), the white outline denotes location of two new aggregates that deposited at the edge of the growing terraces. Image size: 1 [mult] 1 μm. Scan rate: 2.0 Hz.

Czajkowsky et al.; 1998). In the case of crystalline protein complexes, these interactions are expected to vary periodically, reflecting regular variations in surface topography and changes in the local surface characteristics, including charge, of the individual complexes. On the (110) crystal plane, the individual insulin hexamer–protamine complexes are oriented edge-on with the central Zn^{2+} ion channel oriented along the symmetry-equivalent $\langle \bar{1}11 \rangle$ directions. In this orientation, only certain surfaces of the complexes are interrogated by the scanning tip. This was confirmed by superposition of the topography and phase-contrast images that indicated the dark regions on the phase image, corresponding to increased adhesion and energy dissipation, coincided with the interstitial regions between hexamers on the (110) plane. The clear phase and height difference between individual $Lys^{B28}Pro^{B29}$ hexamer–protamine complexes therefore suggests that the observed phase image contrast arises from a combination of viscoelasticity and adhesion, likely due to variations in local surface charge,

between the individual $Lys^{B28}Pro^{B29}$ hexamer–protamine complexes as oriented on the (110) crystal plane.

Crystal growth

Tapping mode AFM performed in crystallization liquor at 33°C before the onset of gross crystal dissolution, revealed gradual expansion of large (110) crystal terraces similar to growth of (001) crystal planes observed previously for other insulin forms. (Fig. 3 A) (Yip and Ward, 1996; Yip et al., 1998a,b). However, in situ imaging performed at 6°C revealed rapid 2D nucleation (Volmer–Weber growth) on the large (110) crystal terraces (Fig. 3 B). In contrast to our earlier AFM studies of $Lys^{B28}Pro^{B29}$, no screw dislocations were observed on the actively growing crystal surfaces at either imaging temperature (Yip et al., 1998a). The observation of Volmer–Weber growth at low temperature is not unexpected because the supersaturation and rate of nucleation increase with decreasing temperature. This is consis-

tent with the qualitative observation that crystallization of NPL at reduced temperatures affords small, highly facetted and fragmented crystals (Fig. 1).

Sequential AFM images acquired at 6°C over extended periods revealed active adsorption and desorption of 17-Å-tall aggregates on the exposed (110) plane of the NPL crystals (Fig. 4). Although the scanning motion of the AFM tip may enhance growth by increasing convection near the sample surface, we did not observe tip-induced nucleation events or tip-induced direct incorporation of aggregates into the crystal terraces. Unambiguous identification of the 17-Å-tall aggregates is difficult because there are two distinct molecular species, $Lys^{B28}Pro^{B29}$ and protamine, in the crystallization liquor. The 17-Å height is incommensurate with the 44-Å terrace heights, and somewhat smaller than the insulin hexamer aggregates reported in our earlier studies (Yip and Ward, 1996; Yip et al., 1998a,b). Although the shape and dimensions of the AFM tip can contribute to an overestimation of lateral feature size, the observed vertical dimensions generally are immune to such effects (Möller et al., 1999). Because NPL crystallization is performed in the presence of phenol and zinc, it is likely that $Lys^{B28}Pro^{B29}$ exists in a hexameric form, although the existence of a small population of $Lys^{B28}Pro^{B29}$ monomers cannot be discounted. However, NPL crystallizes at pH 7.3, which is slightly greater than the reported point of zero charge (6.0–7.0) for NPL (DeFelippis et al., 1998). This would favor adsorption of positively charged protamine molecules (pI = 13.8, Hoffman et al., 1990) through electrostatic interactions onto the negatively charged NPL crystal surface. We note that previous isothermal calorimetry studies described the electrostatic binding of hexameric human insulin to the surface of NPH crystals in a similar fashion (Dodd et al., 1995). These considerations argue that the small features described above are likely protamine aggregates. Epitaxial assembly of protamine on the exposed surface of the NPL crystals is unlikely because the crystal structure of the related NPH complex revealed that the protamine molecules are intertwined within the individual insulin hexamers and are not freely exposed on any crystal planes (Balschmidt et al., 1991). This contrasts with our earlier studies that revealed the epitaxial assembly of aggregates, presumably insulin hexamers, on actively growing insulin crystal surfaces (Yip and Ward, 1996; Yip et al., 1998a,b).

The present studies demonstrate further that low temperature TMAFM performed in solution enables the direct assessment of the interfacial structure, morphology, and crystal growth characteristics for crystalline protein complexes. This approach enabled direct determination of molecular packing on exposed crystal planes by both conventional height and phase imaging, the latter reflecting differences in the local energy dissipation arising from the interaction of the tapping tip with the surface of the protein crystal. Phase imaging clearly revealed periodicities consistent with the arrangement of individual $Lys^{B28}Pro^{B29}$ hex-

amer–protamine complexes, thus enabling direct in situ identification of specific lattice periodicities and plane group symmetries. These observations also illustrate that AFM phase imaging will become increasingly useful for high-resolution electrostatic mapping of domains within biomolecular complexes.

REFERENCES

Baker, E. N., and G. G. Dodson. 1970. X-ray diffraction data on some crystalline varieties of insulin. *J. Mol. Biol.* 54:605–609.

Bakaysa, D. L., J. Radziuk, H. A. Havel, M. L. Brader, S. L. Edwards, S. W. Dodd, J. M. Beals, A. H. Pekar, and D. N. Brems. 1996. Physiochemical basis for the rapid time-action of $Lys^{B28}Pro^{B29}$–insulin: dissociation of a protein-ligand complex. *Protein Sci.* 5:2521–2531.

Balschmidt, P., F. B. Hansen, E. F. Dodson, G. G. Dodson, and F. Korber. 1991. Structure of porcine insulin cocrystallized with clupeine Z. *Acta Cryst.* B47:975–986.

Banting, F. G., and C. H. Best. 1922. Pancreatic extracts. *J. Lab. Clin. Med.* 7:464–472.

Birnbaum, D. A., M. A. Kilcomons, M. R. DeFelippis, and J. M. Beals. 1997. Assembly and dissociation of human insulin and $Lys^{B28}Pro^{B29}$–insulin hexamers: a comparison study. *Pharm. Res.* 14: 25–36.

Brandsch, R., G. Bar, and M.-H. Whangbo. 1997. On the factors affecting the contrast of height and phase images in tapping mode atomic force microscopy. *Langmuir.* 13:6349–6353.

Brange, J., G. G. Dodson, and B. Xiao. 1991. Designing insulin for diabetes therapy by protein engineering. *Curr. Opin. Struct. Biol.* 1:934–940.

Brange, J. Galenics of Insulin: The Physico-Chemical, and Pharmaceutical Aspects of Insulin, and Insulin Preparations. Springer-Verlag, Berlin, Heidelberg, 1987.

Brems, D. N., L. A. Alter, M. J. Beckage, R. E. Chance, R. D. DiMarchi, L. K. Green, H. B. Long, A. H. Pekar, J. E. Shields, and B. H. Frank. 1992. Altering the association properties of insulin by amino acid substitution. *Protein Eng.* 5:527–533.

Brems, D. N., P. L. Brown, L. A. Hekenlaible, and B. H. Frank. 1990. Equilibrium denaturation of insulin and proinsulin. *Biochemistry.* 29: 9289–9293.

Bryant, C., M. Strohl, K. Green, H. B. Long, L. A. Alter, A. H. Pekar, R. E. Chance, and D. N. Brems. 1992. Detection of an equilibrium intermediate in the folding of a monomeric insulin analog. *Biochemistry.* 31: 5692–5698.

Carter, P. W., A. C. Hillier, and M. D. Ward. 1994. Nanoscale surface topography and growth of molecular crystals: the role of anisotropic intermolecular bonding. *J. Am. Chem. Soc.* 116:944–953.

Ciszak, E., J. M. Beals, B. H. Frank, J. C. Baker, N. D. Carter, and G. D. Smith. 1995. Role of C-terminal B-chain residues in insulin assembly: the structure of hexameric $Lys^{B28}Pro^{B29}$–human insulin. *Structure.* 3:615–622.

Cleveland, J. P., B. Anczykowski, A. E. Schmid, and V. B. Elings. 1998. Energy dissipation in tapping mode atomic force microscopy. *Appl. Phys. Lett.* 72:2613–2615.

Czajkowsky, D. M., M. J. Allen, V. Elings, and Z. F. Shao. 1998. Direct visualization of surface charge in aqueous solution. *Ultramicroscopy.* 74:1–5.

DeFelippis, M. R., D. L. Bakaysa, M. A. Bell, M. A. Heady, S. Li, S. Pye, K. M. Youngman, J. Radziuk, and B. H. Frank. 1998. Preparation and characterization of a cocrystalline suspension of [LysB28,ProB29]–human insulin analogue. *J. Pharm. Sci.* 87:170–176.

DiMarchi, R. D., J. P Mayer, L. Fan, D. N. Brems, B. H. Frank, L. K. Green, J. A. Hoffman, D. C. Howey, H. B. Long, W. N. Shaw, J. E. Shields, L. J. Slieker, K. S. E. Su, K. L. Sundell, and R. E. Chance. 1992. Synthesis of fast acting insulin based on structural homology with insulin-like growth factor I. *In* Peptides: Chemistry and Biology, Proceedings of the Twelfth American Peptide Symposium, J. E. Smith and J. E. Rivier (eds.). ESCOM, Leiden, The Netherlands. 26–28.

Dodd, S. W., H. A. Havel, P. M. Kovach, C. Lakshminarayan, M. P. Redmon, C. M. Sargeant, G. R. Sullivan, and J. M. Beals. 1995. Reversible adsorption of soluble hexameric insulin onto the surface of insulin crystals cocrystallized with protamine: an electrostatic interaction. *Pharm. Res.* 12:59–67.

Durbin, S. D., and W. E. Carlson. 1992. Lysozyme crystal growth studied by atomic force microscopy. *J. Cryst. Growth.* 122:71–79.

Durbin, S. D., W. E. Carlson, and M. T. Saros. 1993. In situ studies of protein crystal growth by atomic force microscopy. *J. Phys. D: Appl. Phys.* 26:B128–B132.

Fullerton, W. W., and B. W. Low. 1970. Insulin crystallization in the presence of basic proteins and peptides. *Biochim. Biophys. Acta.* 214:141–147.

Goldman, J., and F. H. Carpenter. 1974. Zinc binding, circular dichroism, and equilibrium sedimentation studies on insulin (bovine) and several of its derivatives. *Biochemistry.* 13:4566–4574.

Hagedorn, H. C., B. N. Jensen, N. B. Krarup, and I. Woodstrup. 1936. Protamine insulin. *JAMA.* 106:177–180.

Hillier, A. C., and M. D. Ward. 1994. Atomic force microscopy of the electrochemical nucleation and growth of molecular crystals. *Science.* 263:1261–1264.

Hoffman, J. A., R. E. Chance, M. G. Johnson, and R. E. Hoffmann. 1990. Purification and analysis of the major components of chum salmon protamine contained in insulin formulations using high performance liquid chromatography. *Protein Expr. Purif.* 1:127–133.

Hollenberg, M. D. 1990. Receptor triggering and receptor regulation: structure-activity relationships from the receptor's point of view. *J. Med. Chem.* 33:1275–1281.

Konnert, J. H., P. D'Antonio, and K. B. Ward. 1994. Observations of growth steps, spiral dislocations and molecular packing on the surface of lysozyme crystals with the atomic force microscope. *Acta Cryst.* D50:603–613.

Krayenbuhl, C., and T. Rosenberg. 1946. Crystalline protamine insulin. *Rep. Steno. Mem. Hosp. Nord. Insulinlab.* 1:60–73.

Land, T. J., A. J. Malkin, Y. G. Kutznesov, A. McPherson, and J. J. DeYoreo. 1996. Mechanisms of protein and virus crystal growth: an atomic force microscopy study of canavalin and STMV crystallization. *J. Crystal Growth.* 166:893–899.

Land, T. J., A. J. Malkin, Y. G. Kuznetsov, A. McPherson, and J. J. De Yoreo. 1995. Mechanisms of protein crystal growth: an atomic force microscopy study of canavalin crystallization. *Phys. Rev. Lett.* 75:2774–2777.

Li, H., M. A. Perozzo, J. H. Konnert, A. Nadarajah, and M. L. Pusey. 1999. Determining the molecular-packing arrangements on protein crystal faces by atomic force microscopy. *Acta Cryst. D.* 55:1023–1035.

Li, H., A. Nadarajah, and M. L. Pusey. 1999. Determining the molecular-growth mechanisms of protein crystal faces by atomic force microscopy. *Acta Cryst. D.* 55:1036–1045.

Long, H. B., J. C. Baker, R. M. Belagaje, R. D. DiMarchi, B. H. Frank, L. K. Green, J. A. Hoffman, W. L. Muth, A. H. Pekar, S. G. Reams, W. N. Shaw, J. E. Shields, L. J. Slieker, K. S. E. Su, K. L. Sundell, and

R. E. Chance. 1992. Human insulin analogs with rapid onset and short duration of action. *In* Peptides: Chemistry and Biology, Proceedings of the Twelfth American Peptide Symposium, J. E. Smith and J. E. Rivier (eds.). ESCOM, Leiden, The Netherlands. 88–90.

Magonov, S. N., V. Elings, and M.-H. Whangbo. 1997. Phase imaging and stiffness in tapping-mode atomic force microscopy. *Surf. Sci. Lett.* 375:L385–L391.

Malkin, A. J., T. J. Land, Y. G. Kuznetsov, A. McPherson, and J. J. De Yoreo. 1995. Investigation of virus crystal growth mechanisms by in-situ atomic force microscopy. *Phys. Rev. Lett.* 75:2778–2781.

Malkin, A. J., Y. G. Kuznetsov, and A. McPherson. 1996. Defect structure in macromolecular crystals. *J. Struct. Biol.* 117:124–137.

McPherson, A., A. J. Malkin, Y. G. Kuznetsov, and S. Koszelak. 1996. Incorporation of impurities into macromolecular crystals. *J. Cryst. Growth.* 168:74–92.

Möller, C., M. Allen, V. Elings, A. Engel, and D. J. Müller. 1999. Tapping-mode atomic force microscopy produces faithful high-resolution images of protein surfaces. *Biophys. J.* 77:1150–1158.

Muller, D. J., G. Buldt, and A. J. Engel. 1995. Force-induced conformational change of bacteriorhodopsin. *Mol. Biol.* 249:239–243.

Ng, J. D., Y. G. Kuznetsov, A. J. Malkin, G. Keith, R. Giege, and A. McPherson. 1997. Visualization of RNA crystal growth by atomic force microscopy. *Nucleic Acid Res.* 25:2582–2588.

Noy, A., C. H. Sanders, D. V. Vezenov, S. S. Wong, and C. M. Lieber. 1998. Chemically-sensitive imaging in tapping mode by chemical force microscopy: Relationship between phase lag and adhesion. *Langmuir.* 14:1508–1511.

Pekar, A. H., and B. H. Frank. 1972. Conformation of proinsulin. A comparison of insulin and proinsulin self-association at neutral pH. *Biochemistry.* 11:4013–4016.

Simkin, R. D., S. A. Cole, H. Ozawa, P. Magdoff-Fairchild, P. Eggena, A. Rudko, and B. W. Low. 1969. Precipitation and crystallization of insulin in the presence of lysozyme and salmine. *Biochim. Biophys. Acta.* 200:385–394.

Smith, G. D., D. C. Swenson, E. J. Dodson, G. G. Dodson, and C. D. Reynolds. 1984. Structural stability in the 4-zinc human insulin hexamer. *Proc. Natl. Acad. Sci. USA.* 81:7093–7097.

Spatz, J. P., S. Sheiko, M. Möller, R. G. Winkler, P. Reineker, and O. Marti. 1995. Forces affecting the substrate in resonant tapping force microscopy. *Nanotechnology.* 6:40–44.

Walz, T., P. Tittmann, K. H. Fuchs, D. Müller, D. L. Smith, P. Agre, H. Gorss, and A. Engel. 1996. Surface topographies at subnanometer-resolution reveal asymmetry and sidedness of aquaporin-1. *J. Mol. Biol.* 264:907–918.

Weiler, J. M., P. Freiman, M. D. Sharath, W. J. Metzger, J. M. Smith, H. B. Richerson, Z. K. Ballas, P. C. Halverson, D. J. Shulan, S. Matsuo, and R. L. Wilson. 1985. Serious adverse reactions to protamine sulfate: are alternatives needed? *J. Allergy Clin. Immunol.* 75:297–303.

Winkler, R. G., J. P. Spatz, S. Sheiko, M. Möller, P. Reineker, and O. Marti. 1996. Imaging material properties by resonant tapping-force microscopy: a model investigation. *Phys. Rev. B.* 54:8908–8912.

Yip, C. M., and M. D. Ward. 1996. Atomic force microscopy of insulin single crystals: direct visualization of molecules and crystal growth. *Biophys. J.* 71:1071–1078.

Yip, C. M., M. L. Brader, M. D. Ward, and M. R. DeFelippis. 1998a. Crystal packing and interfacial structure of crystalline wild-type and analog insulins by atomic force microscopy. Effect of sequence variation on hexamer self-assembly. *Biophys. J.* 74:2199–2209.

Yip, C. M., M. R. DeFelippis, B. H. Frank, M. D. Ward, and M. L. Brader. 1998b. Structural and morphological characterization of ultralente insulin crystals by atomic force microscopy: evidence of hydrophobically driven assembly. *Biophys. J.* 74:1172–1179.

Zhang, Y., S. Sheng, and Z. Shao. 1996. Imaging biological structures with the cryo atomic force microscope. *Biophys. J.* 71:2168–2176.